MODIFICATION OF OPTICAL PROPERTIES OF POROUS $A^{III}B^{V}$ LAYERS PRODUCED BY ANODIC ETCHING

N. DMITRUK,[1] N. BEREZOVSKA,[2] I. DMITRUK,[2] V. SERDYUK,[1] J. SABATAITYTE,[3] I. SIMKIENE[3]

[1]**V.E. Lashkaryov Institute of Semiconductor Physics, Nat. Acad. of Sci. of Ukraine**
(41, Prosp. Nauky, Kyiv 03028, Ukraine)

[2]**Taras Shevchenko National University of Kyiv**
(64, Volodymyrs'ka Str., Kyiv 01601, Ukraine)

[3]**Semiconductor Physics Institute**
(11, Gostauto, Vilnius 01108, Lithuania)

Morphology investigations (atomic force microscopy (AFM) and scanning electron microscopy (SEM)), study of Raman scattering (RS) and photoluminescence (PL) have been performed to characterize a series of $A^{III}B^{V}$ materials (GaAs, GaP, InP) with an electrochemically prepared porous surface layer. It has been shown that the surface morphology of porous $A^{III}B^{V}$ compounds strongly depends on various parameters of the anodization process such as the etching time, current density, composition of etching solution, and illumination during the etching procedure. The enhancement of a Raman signal from porous surfaces, which has been observed for almost all samples, is caused mainly by the breaking of selection rules for corresponding phonon modes and a decrease of the reflection at the porous surface. The peculiarities of the PL spectra of porous $A^{III}B^{V}$ compounds are studied in a wide temperature range. The small quantum confinement effect has been observed for GaAs and InP porous surfaces.

1. Introduction

In recent years, the technology of nano-sized semiconductors presents a rapidly developing field in materials science because of the particular physical and chemical properties of semiconductor nanostructures, which are perspective for various applications. Porous polar semiconductor compounds $A^{III}B^{V}$ have mainly a direct band gap and a large refractive index, which is of great importance for applications in photonics and standard and polaritonic optoelectronics. Porous compounds of the $A^{III}B^{V}$ type, especially GaAs, InP, GaP, and GaN, provide a broad elemental basis for the research of electron and phonon excitations. Besides optoelectronic applications, these materials are perspective for the photoelectric devices and solar cells due to antireflecting and isolating properties, in sensorics due to the large surface-to-volume ratio, and in nanophotonics due to the large birefringence.

The important peculiarity of the surface electron properties of $A^{III}B^{V}$ semiconductors is the existence of a depletion layer on the semiconductor/native oxide interface due to the corresponding spectrum of surface electron states [1]. The preparation of the porous surface allows one to minimize the density of surface electron states attenuating the radiative recombination (luminescence) and the intensity of various non-equilibrium (photoelectric) phenomena. It is known that many efforts have been applied to prepare porous surface layers (micro-, meso-, macro-) in $A^{III}B^{V}$ semiconductors (see reviews [2, 3]) by the anodic etching. Earlier, this technique usually was used for the isotropic polishing etching under conditions of the intensive hole generation provided with powerful illumination. In dark or under enough weak illumination, the chemical dissolution of a semiconductor starts at some active surface points. Therefore, a system of pores oriented along some crystallographic direction or along the current lines can be prepared [4].

It should be noted that the electrochemical formation of pores is an extreme case of the anisotropic wet chemical etching, which is widely used in the fabrication of devices [5, 6]. For $A^{III}B^{V}$ semiconductor compounds (GaAs, InP, InAs, GaP, GaSb, *etc.*), many effective methods of electrochemical etching have been elaborated [2, 3, 7–10]. In addition, the electrochemical method for microrelief (porous) surface preparation allows one to change the statistical geometrical parameters of a surface microrelief in a wide range.

This paper presents the comprehensive study of the surface morphology and peculiarities of the phonon-plasmon interaction and the secondary photon emission of GaAs, InP, GaP porous layers obtained by the electrochemical etching.
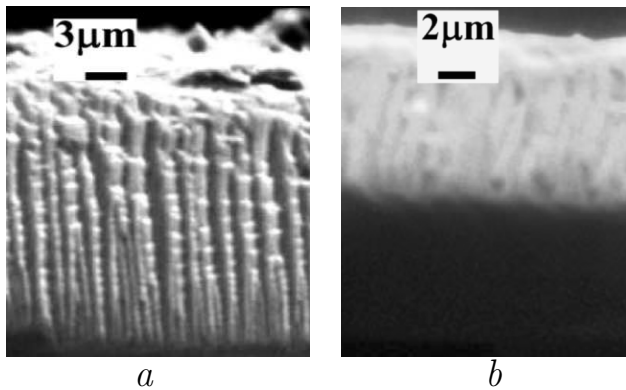
Fig. 1. SEM images of cleaved border edges of samples n-GaAs No. 7 illuminated from top (a) and bottom (b) during the anodization

Fig. 2. SEM top view of n-GaAs samples obtained a) at a low current density (sample No. 1) and b) at a high current density (sample No. 4)

2. Preparation and Morphology of Porous Layers

A simple cheap technology of electrochemical etching, as one of the most versatile techniques for the fabrication of large-area nano-sized crystalline or porous materials, is used for the preparation of the samples studied in the present paper.

In our case, the substrates were n-type semiconducting wafers. Before the etching, the samples have been placed in an ultrasound bath, degreased by treatment with acetone, isopropanol, and ethanol, and afterward rinsed with distilled water. The subsequent etching in an $NH_4OH:H_2O:H_2O_2$ (3:400:1) solution for 30 s and the cleaning for about two minutes in $HCl:H_2O$ (1:1) were performed to remove the oxide film formed in air. The back contact to wafers was made by smearing In/Ga alloy onto samples. A Pt plate was employed as a cathode. During the electrochemical etching procedure, the wafers were illuminated by an incandescent lamp providing the light flux of 600–1200 Lx from the top or from the bottom of the etched substrates in order to generate additional charge carriers (holes) at semiconductor surfaces. The GaP samples were in dark during the anodization. The parameters of samples and technology conditions are presented in Table.

The morphology of the obtained samples was studied by a scanning electron microscope (SEM) BS300 in the electron beam induced current (EBIC) mode and in the secondary electron imaging mode (with a primary beam energy up to 26 keV). An atomic force microscope (AFM) Dimension 3100 (Digital Instruments) was also used to investigate the surface morphology.

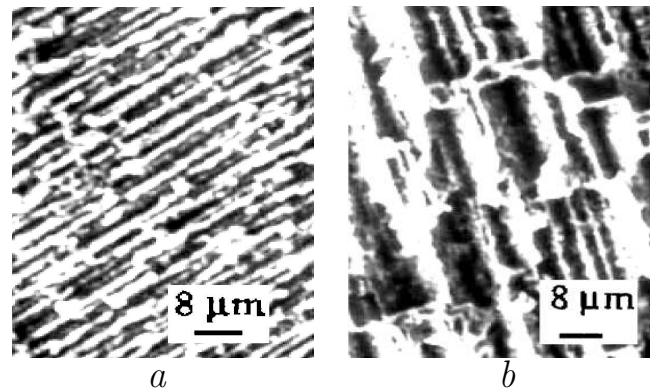The two-layer structure of porous layers of GaAs samples was found, by using the SEM investigations (see

the SEM picture of the sample cross-section, Fig. 1,a,b). The top layer primarily consists of As_2O_3, Ga_2O_3, and GaAs nanocrystals, as was shown in [11–13]. The bottom layer with pores of different sizes depending on the substrate resistance and etching conditions was formed on the surface of a monocrystalline substrate. The surface morphology strongly depends on the current density and illumination during the etching procedure. For GaAs samples at the lowest current density (4 mA/cm^2 – sample No. 1), the structure consists of macrorods ($\sim$1 μm in width) and pores ($\sim$ 20 μm in depth) (Fig. 2,a). At high current density (sample No. 4), the characteristic size of the surface structure increases (Fig. 2,b).

Samples data

Sample specification	Technological parameters		
	Etchant composition	Current density, mA/cm^2	Etching time, min
GaAs, n-type: 10^{17}–10^{18} cm^{-3}, (100)			
No. 1	1 M HCl	4	10
No. 4	1 M HCl	30	10
No. 6	1 M HCl	10	20
No. 7	1 M HCl	5	20
No. 8	1 M HCl	20	10
GaP, n-type: (2.5–3) $\times 10^{18}$ cm^{-3}, (111)			
No. 1	0.5 M H$_2$SO$_4$	10	10
No. 2	0.5 M H$_2$SO$_4$	5	20
InP, n-type: $\sim 10^{18}$ cm^{-3}, (100)			
No. 22	1 M HCl	5	30
No. 23	1 M HCl	2	5
No. 28	1 M HCl	3	5
No. 30	1 M HCl	5	3
No. 32	1 M HCl	1	10

Fig. 3. AFM images of the porous surface of n-GaP (111) samples No. 1 (a) and No. 2 (b), respectively
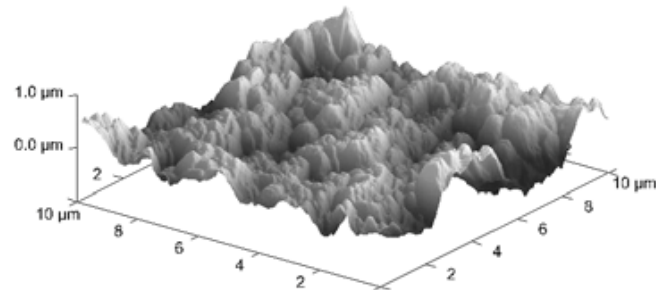

Fig. 4. AFM image of the porous surface of n-InP sample No. 30

of pores depends on the current density: the larger the current density, the larger the diameter of pores. The porous layer with macropores and grains of up to 1 μm was formed at a higher current density and a shorter anodization time (Fig. 3,a). The pores and grains are irregularly distributed in the lateral plane. As the etching time increases, the morphology of the porous structure changes, and the pore density increases (Fig. 3,b).

In this paper, we have investigated n-InP samples electrochemically etched in the galvanostatic regime. The surface structures are oriented along crystallographic axes. The two-layer structure of porous InP was observed (Fig. 4). The top layer a few micrometers in thickness consists of native oxides and reaction products. We have discussed previously [15] that porous GaP and InP layers are much less oxidized by the etching than GaAs layers. The bottom layer is porous InP and consists of macrorods. In common with other studied $A^{III}B^V$ compounds, the tendency to the formation of pores with larger diameter at a larger current density has been also observed for InP samples.

The thickness of the porous layer illuminated from the top of the sample is larger than the one illuminated from the bottom (see Fig. 1). The morphology of porous layers depends also on the type and the concentration of an electrolyte, primarily, on its content. Formerly, we have investigated the porous n-type GaAs layers obtained with $HF:C_2H_5OH:H_2O$ electrolyte [10, 14, 15].

The H_2SO_4–based electrolytes were often used for the formation of porous GaP layers by the electrochemical technique at constant high (up to 20 V) external potentials (potentiostatic regime). It was determined [16] that, under these etching conditions, SO_4^{2-} ions took part in both formation and dissolution of oxides. As a result, upper porous layers did not form. In contrast, we used the galvanostatic regime in the same H_2SO_4–based electrolyte to form porous GaP layers. The morphology of porous GaP is illustrated in Fig. 3. The diameter

3. Results and Discussion

3.1. Raman scattering spectroscopy

Raman spectroscopy has been used for the characterization of a modification of $A^{III}B^V$ semiconductor materials after the electrochemical etching. The study of peculiarities of the Raman spectra of porous layers is significant for the control and the optimization of the layer formation process. The position of optical phonon bands and their width and shape make it possible to characterize structural peculiarities of the porous layer. The analysis of coupled phonon-plasmon modes allows us to estimate the carrier concentration and the carrier mobility. In this paper, we present the most interesting Raman spectra obtained for different samples.

Raman scattering measurements were performed, by using an optical setup made on the basis of a DFS-24
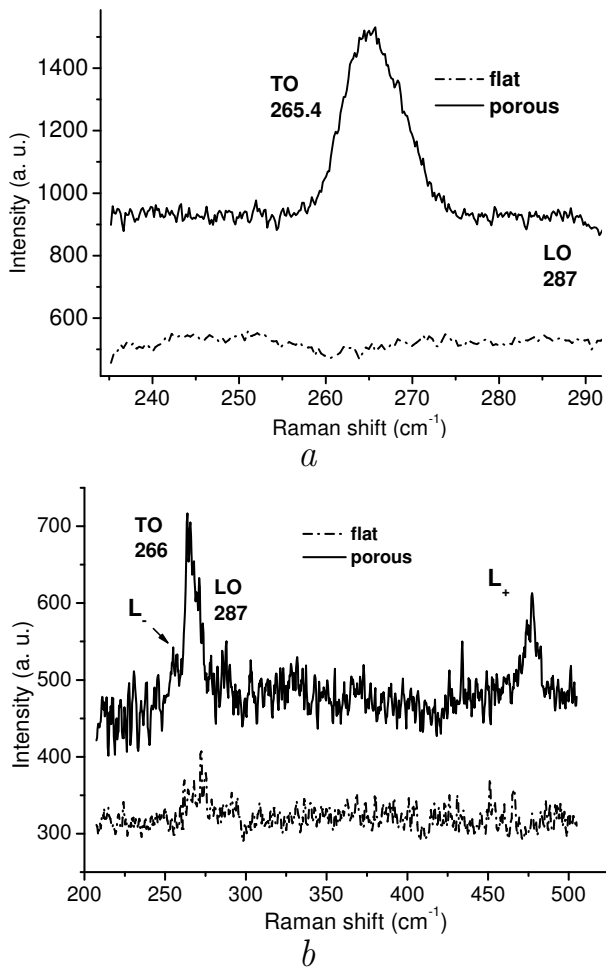
Fig. 5. Raman spectra of n-type GaAs samples No. 6 (a) and No. 7 (b) at room temperature, $\lambda_{\mathrm{exc}} = 514.5$ nm

double-grating monochromator. Raman spectra were measured at room temperature with s-polarized Ar-laser light with a wavelength of 488 or 514.5 nm at the incidence angle $\varphi = 45°$. The scattered light was collected at the normal to the sample surface, i.e. in the quasibackscattering geometry.

The Raman spectra of the porous n-GaAs (100) surfaces contain bands which can be related to the transversal optical (TO) phonon (~ 266 cm^{-1}) mode and the longitudinal optical (LO) phonon (~ 287 cm^{-1}) one. According to the selection rules for the Raman scattering in a GaAs crystal and for our geometry of the experiment (quasibackscattering geometry), only the LO mode should be observable at the (100) surface orientation. In the Raman spectra of a porous layer for the majority of GaAs samples, the TO mode has been revealed (see Fig. 5). As compared to the samples studied in [14], the

intensity of the TO mode has been considerably larger than that for the LO mode. The enhancement of the surface scattering was observed in the most porous samples of GaAs. The appearance of the forbidden TO mode is caused by the violation of the selection rules for the TO mode at (100) orientation. In general, the appearance of these phonons may be due to several reasons, namely the distortion of the back-scattering geometry due to a particular experimental geometry, a disorder of crystallographic orientations in the walls of the porous layer (skeleton), the appearance of defects in the crystal lattice, and the influence of the surface electric field in the lateral surfaces of pores on the selection rules for the macroscopic symmetry of a porous crystal.

Both TO- and LO-phonons demonstrate a more or less pronounced low-frequency shift of about $1 \div 2$ cm^{-1} on the porous surfaces of some samples. It can be attributed to the quantum-size effect on the phonons in GaAs nanocrystals [14, 17].

The sufficiently intense band (L$_+$) has been observed in the high-frequency region of the Raman spectrum of doped GaAs (Fig. 5,b). The presented Raman spectrum has also another feature (L$_-$) at 255 cm^{-1}. These bands are caused by the interaction of fluctuations of the free carriers charge density with the macroscopic longitudinal electric field of LO optical vibrations of the GaAs lattice. Thus, the presence of two peaks with frequencies $\omega_+ > \omega_{\mathrm{LO}}$ (L$_+$-mode) and $\omega_- < \omega_{\mathrm{TO}}$ (L$_-$-mode) indicates the plasmon-phonon interaction at the comparable values of plasmon and LO-phonon frequencies, and $\Gamma_p \ll \omega_p$, where Γ_p is the damping of plasmons, and ω_p is the plasma frequency. The experimental values of frequencies of optical phonons, coupled phonon-plasmon modes, and literature values of carrier effective masses and high-frequency dielectric constant [18, 19] allowed us to specify the carrier concentration for this sample $n \sim 1.6 \times 10^{18}$ cm^{-3}.

The intense bands in the Raman spectra of both porous and flat surfaces of n-GaP (111) are the TO (~ 366 cm^{-1}) and LO (~ 404 cm^{-1}) phonon modes (Fig. 6,a). Surface phonons were hardly observed on the low-frequency wing of the LO mode. The second-order Raman spectra at ~ 722–786 cm^{-1} with the intensity by about two orders smaller correspond to maxima of the combined density of states of pairs of phonons 2TO, TO+LO, and 2LO (Fig. 6,b).

In the Raman spectra of some samples (for example, sample No. 2), the difference between the TO and LO modes (~ 38 cm^{-1}) is slightly less (by ~ 0.5 cm^{-1}) for the porous surface, as compared with the flat one. This

effect is more pronounced in the second-order Raman spectra.

A possible explanation of the reduced LO-TO splitting for porous materials can be suggested from the effective-medium approach in the upper Wiener limit [20]. Due to a considerable fraction of voids, the dielectric constants of material ε_0 and ε_∞ decrease, and their ratio which determines the LO-TO splitting decreases.

In addition, the LO-TO splitting decrease means a decrease of the polar oscillator strength, $\rho = (\varepsilon_\infty/4\pi)(\omega_{\rm LO}^2/\omega_{\rm TO}^2 - 1)$, due to a distortion of the geometric structure during the electrochemical etching. This is confirmed also by the reflectance decrease in the reststrahlen region, $\omega_{\rm T} \div \omega_{\rm L}$.

Under these conditions, the observation of surface phonons should be improved. However, we did not reveal distinctly these surface modes in porous GaP. May be, this is determined by the back-scattering geometry of our Raman scattering measurements, because the forward scattering geometry is preferable for the observation of surface phonons [21].

The Raman spectra of porous InP samples are very similar to GaAs, but the relative intensity of phonon bands is lower. We observe an enhancement of the Raman signal from porous layers by several orders of magnitude (Fig. 7,a). Possible reasons for this enhancement could be a decrease of the reflection on the porous surface and the breaking of selection rules at the disordered surface. However, probably, the above-mentioned causes cannot explain the observed strong enhancement by more than one order of magnitude.

The second-order Raman spectrum of the porous surface of n-InP (100) (sample No. 30) observed at ~ 618–688 cm^{-1} is caused by overtones and combined frequencies of optical phonons (Fig. 7,c). Another prominent band at 930 cm^{-1} in the spectrum can be attributed to the coupled LO-phonon-plasmon mode L_+. The second coupled LO-phonon-plasmon mode L_- has not been observed evidently in the spectrum (see Fig. 7,b). It should be at 301–302 cm^{-1} in view of a carrier concentration of 7.1×10^{18} cm^{-3} for an n-InP wafer. The position of the L_+ mode indicates that the carrier density in the porous layer approximately reduces to 6.9×10^{18} cm^{-3} in comparison with that of the InP substrate. Such behavior is in accordance with the study of the distribution of free carriers in porous layers of some $\mathrm{A}^{\rm III}\mathrm{B}^{\rm V}$ semiconductors presented in [22, 23].

G. Irmer approved [23] that, as the doping level increases, the wall thickness of the semiconducting skeleton decreases, and the current carrier depletion occurs.
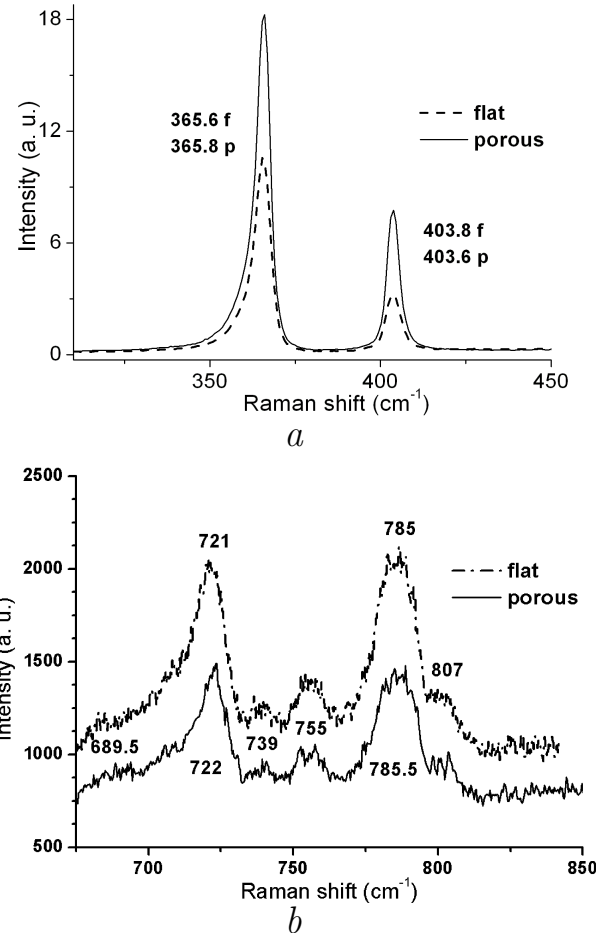

Fig. 6. Raman spectra of porous n-GaP (111) sample No. 1 in the region of the first-order spectrum (a) and sample No. 2 in the region of the second-order spectrum (b) at room temperature, $\lambda_{\rm exc} = 514.5$ nm

The free-carrier concentration of the semiconducting skeleton will be influenced by the depletion layers existing below the surfaces. The mean carrier concentration decreases. G. Irmer stated that, for the concentration $n \sim 2 \times 10^{18}$ cm^{-3}, the skeleton is completely depleted. Instead of the coupled LO phonon-plasmon modes seen in the bulk, the pure LO phonon mode appears. In our case for the InP sample with the concentration $n \sim 7.1 \times 10^{18}$ cm^{-3}, we have seen simultaneously the pure LO mode and L_+ mode. For the InP substrate, we have observed only a weak band in the region of the L_+ mode. The morphology of this sample (see Fig. 4) demonstrates a rather inhomogeneous surface with a system of pores of different dimensions. Possibly, we did not have a sufficient decrease of the free carries concentration that would be resulted in a decrease of the L_+ mode. We note the changes of the Raman spectrum of
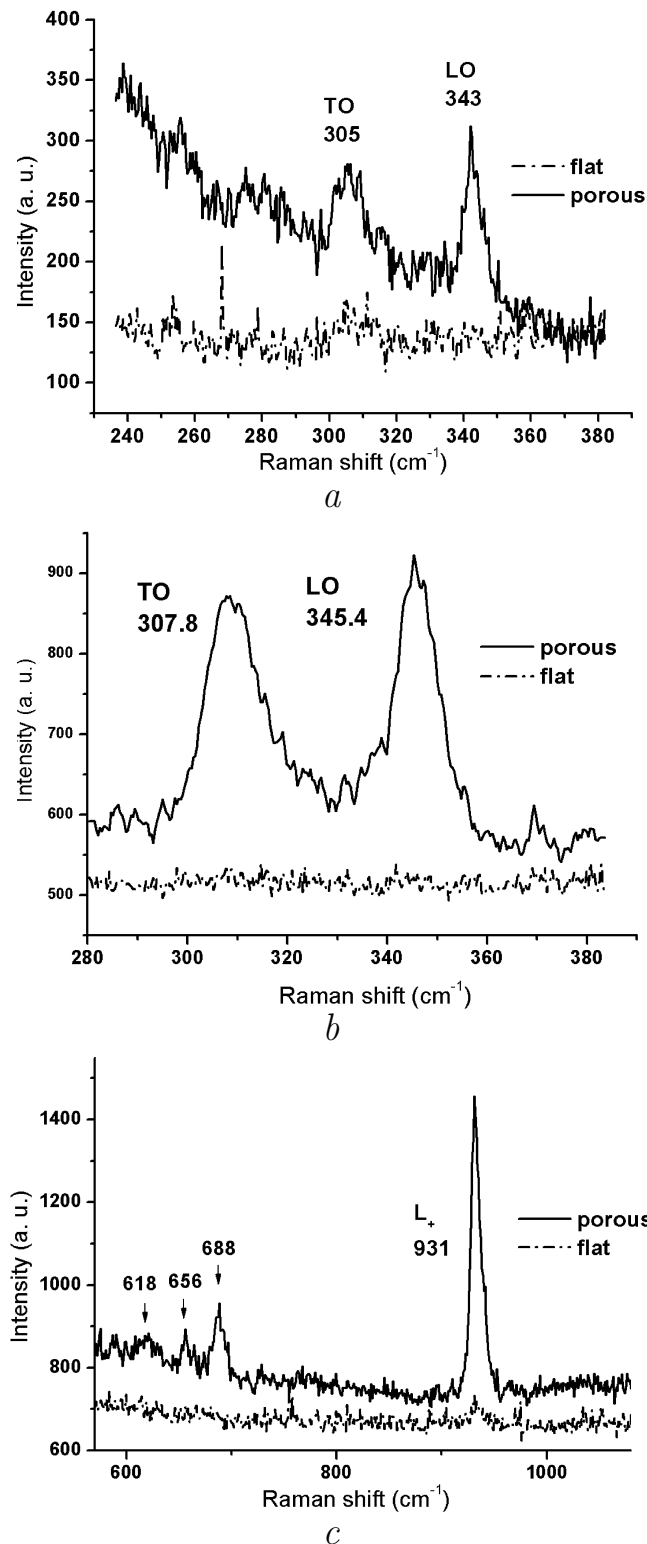
a

b

c

Fig. 7. First-order Raman spectra of *n*-InP samples No. 22 (*a*) and No. 30 (*b*), the high-frequency region of the spectrum for InP sample No. 30 (*c*) at room temperature, $\lambda_{\text{exc}} = 514.5$ nm
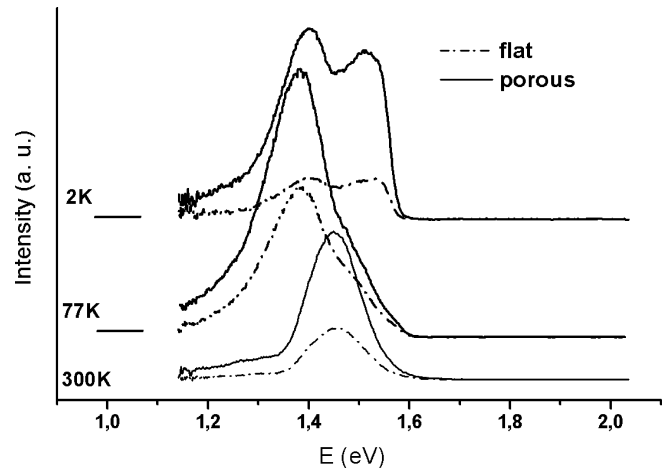

Fig. 8. Photoluminescence spectra of *n*-type GaAs sample No. 8 at different temperatures, $\lambda_{\text{exc}} = 514.5$ nm

a porous InP sample which occurred after some time. Within a year, the intensity of the L_{+} mode sufficiently decreased. The most probable reason for this is the effect of the depletion of the skeleton.

3.2. Photoluminescence spectroscopy

The photoluminescence (PL) spectra of three $A^{\text{III}}B^{\text{V}}$ semiconductor compounds, GaAs, InP, and GaP were measured with a MDR-3 single monochromator at room and low (77 and 2 K) temperatures (Figs. 8–10).

Two bands at 1.51 eV and 1.4 eV have been revealed in the PL spectra of GaAs at a temperature of 2 K. The observed bands can be caused by the recombination of excitons free and localized at the Te donor or at surface states, respectively. The band at 1.51 eV has a high energy shoulder. This high-energy component can be attributed to the recombination of excitons confined in extremely small GaAs nanocrystals. Estimations performed in the effective mass approximation using the equation describing a change of the exciton energy ΔE caused by the quantum confinement of charge carriers [24] gave the value of about 10 nm for the radius of nanocrystals. For the calculations, the values of electron and hole effective masses and the effective Rydberg energy were taken from [19, 25]: $m_e^* = 0.063$, $m_h^* = 0.53$, $E_{\text{Ry}}^* = 4.9$ meV. With increasing temperature up to 77 K, the PL band with a maximum at an energy of 1.38 ÷ 1.41 eV (depending on the sample) becomes dominant in the spectra. This band is characterized by the high-energy shoulder. We can suggest that the free excitons cannot be observable effectively because of the influence of the processes of scattering

by phonons and free charge carriers and, probably, due to the Auger recombination. The observed low-energy PL band reveals the main channel of recombination via surface electron states in this temperature range. Under a further increase of the temperature up to 300 K, the localized excitons are thermally delocalized and induce the photon emission in a vicinity of 1.45 eV.

The PL emission spectra of porous InP demonstrate one band at about 1.35 eV at room temperature, which coincides with the PL spectra of the flat surface (Fig. 9). The microporous relief leads to a decrease of the spectrum intensity due to an increase of the surface recombination rate. The small quantum confinement effect (about 10 meV) has been observed for some samples at 2 K (see, e.g., Fig. 9,a). The comparison of the band full widths at half maximum (FWHM) shown in Fig. 9,b indicates its increase in the case of a porous sample. This may be related to the significant fluctuation of the conduction and valence band extrema caused by the porosity. The formation of porous InP is accompanied by the appearance of surface electron states near the bottom of the conduction band and the top of the valence band. As is known [26–28], the temperature dependence of the photoluminescence in porous InP is very complicated. Namely, two peaks are observed in porous InP: one peak dominating at $T > 150$ K shows a blue shift by about 14 meV in comparison with bulk InP, while the other peak dominating at $T < 120$ K shows a red shift by about 33 meV. The quantum confinement effect is assumed to be the origin of the blue shift, and the red shifted peak is suggested to be due to the radiative recombination via surface electron states [26]. We have observed only a blue shift of the 1.38-eV band at the low temperature $T = 2$ K, and the temperature independence of the band position at higher temperatures ($T = 77$ K and $T = 300$ K) (Fig. 9,a). For another sample No. 32 (Fig. 9,b), we observed no shift at all. This means that the really nonradiative surface recombination is dominating in porous InP samples prepared by the electrochemical treatment.

Technological conditions for one of the samples (InP (100) No. 23) allowed us to obtain a free standing porous layer. It has been shown [29] that the use of porous substrates leads to a significant reduction in the defect density at interfaces, which makes the porous substrate promising for the use during the heteroepitaxial growth of layers at a considerable mismatch of lattice parameters. In [30], a new method of fabrication of free-standing luminescent layers of porous silicon was demonstrated, which forces us to pay attention to peculiarities of such kind of InP samples.
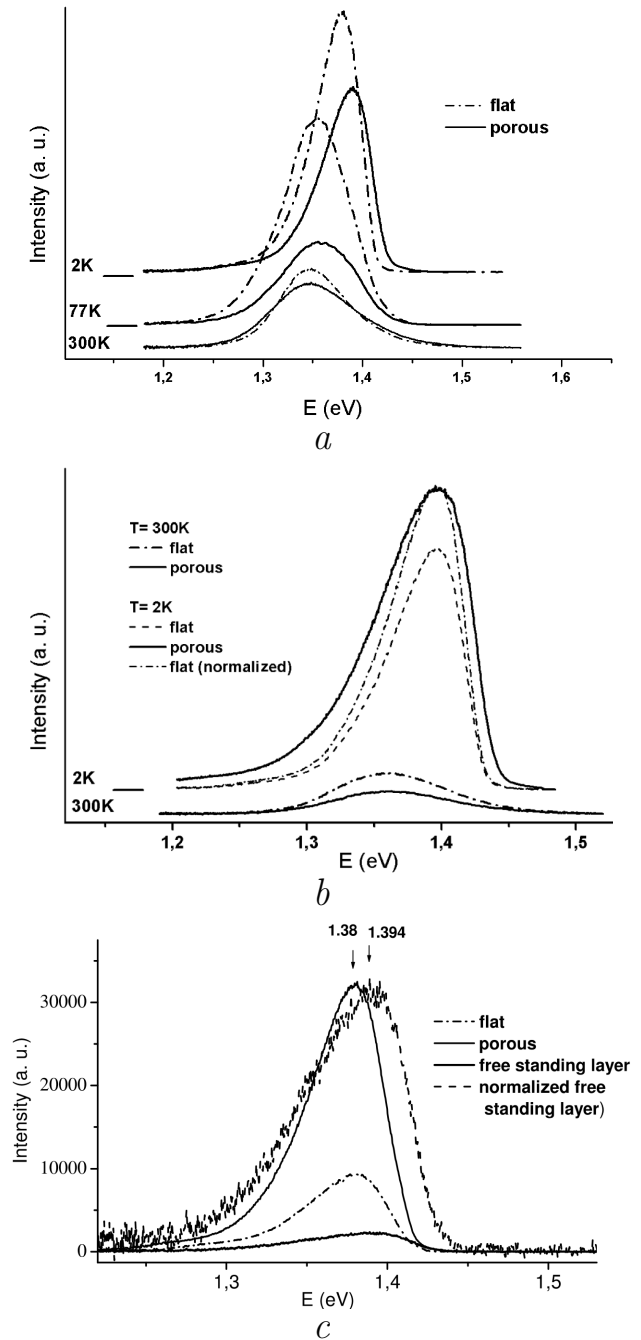

Fig. 9. Photoluminescence spectra of n-type InP samples No. 8 (a), No. 32 (b) at different temperatures and sample No. 23 (c) at $T = 2$ K, $\lambda_{\mathrm{exc}} = 514.5$ nm

In the PL spectrum of sample No. 23 (Fig. 9,c) for the InP free standing porous layer, we observe a PL shift to the high-energy spectral region. This reflects the formation of a layer with ordered thinner skeleton.
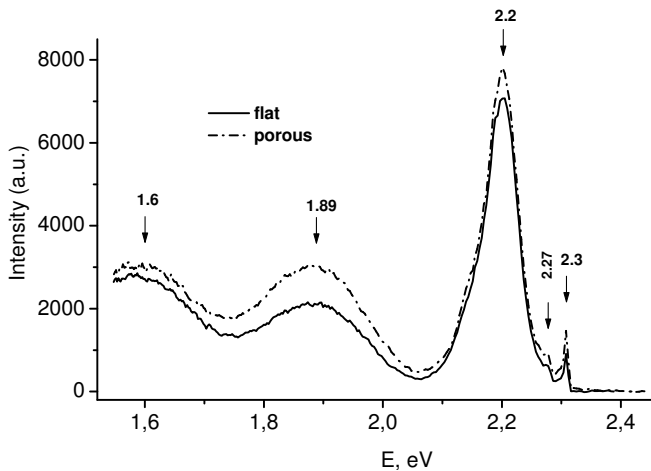
Fig. 10. Photoluminescence spectra of n-type GaP (111) sample No. 2 at $T = 2$ K, $\lambda_{exc} = 488.0$ nm

The photoluminescence spectra of flat and porous GaP are presented in Fig. 10. Unlike other studied $A^{III}B^{V}$ materials, GaP is a semiconductor material with the indirect band gap. Therefore, we could expect the considerable enhancement and quantum size effects in the photoluminescence of the porous surface. Neither was observed. The PL spectrum of the porous surface (Fig. 10) demonstrates only a little increase of the PL amplitude, probably due to a decrease of the reflection. A possible explanation of the absence of the quantum size effects for GaP both in Raman and in photoluminescence spectra is a difference in morphologies. GaP has almost no oxide layer, which could support nanocrystallites obtained in the etching process. Another possible explanation is just a larger size of obtained microstructures.

4. Conclusions

The performed investigations have shown that the surface morphologies of porous $A^{III}B^{V}$ compounds depend strongly on various parameters of the anodization such as the etching time, current density, and composition of an etching solution. The TO-, LO-phonons, surface phonons, and coupled LO-phonon-plasmon modes in the highly doped polar semiconductors GaAs, GaP, and InP have been analyzed. For the porous surfaces, the Raman intensity increase owing to the multiple scattering and the violation of selection rules for optical phonons is confirmed. The LO–TO splitting decreases due to the composite nature of a porous material. In porous layers, the carrier concentration estimated by the position of the coupled LO phonon-plasmon modes is reduced because

of the existence of the surface depletion on the advanced surface of an anodized polar semiconductor. The behavior of the photoluminescence spectra indicates the slight quantum confinement effect for excitons and a change of the surface recombination rate in the GaAs and InP porous compounds.

1. N.L. Dmitruk and V.I. Lyashenko, Fiz. Tverd. Tela **8**, 578 (1966).

2. L. Santinacci and T. Djenizian, C.R. Chimie **11**, 964 (2008).

3. H. Föll, S. Langa, J. Carstensen, M. Christophersen, and I.M. Tiginyanu, Adv. Mater. **15**, 183 (2003).

4. I. Tiginyanu, S. Langa, H. Föll, and V. Ursachi, *Porous III-V Semiconductors: Online Book* (2009) http://www.porous-35.com/index.html.

5. N.L. Dmitruk, T.R. Barlas, and E.V. Pidlisnyi, Surf. Sci. **293**, 107 (1993).

6. N.L. Dmitruk, N.V. Kotova, E.V. Podlisnyi, and T.R. Barlas, Phys. Solid State **35**, 8 (1993).

7. N.L. Dmitruk, O.Yu. Borkovskaya, I.B. Mamontova, and S.V. Mamykin, Sol. Energ. Mat. Sol. C **60**, 379 (2000).

8. P.H.L. Notten, J.E.A.M. van den Meerakker, and J.J. Kelly, *Etching of III-V Semiconductors: An Electrochemical Approach* (Elsevier, Oxford, 1991).

9. J. Sabataityte, I. Simkiene, A.N. Baranov, R. A. Bendorius, and V. Pacebutas, Mater. Sci. Eng. C **23**, 43 (2003).

10. J. Sabataityte, I. Simkiene, R.-A. Bendorius, K. Grigoras, V. Jasutis, V. Pacebutas, H. Tvardauskas, and K. Naudzius, Mater. Sci. Eng. C *19*, 155 (2002).

11. D.J. Lockwood, P. Schmuki, H.J. Labbe, and J.W. Fraser, Physica E **4**, 102 (1999).

12. C.M. Finnie and P.W. Bohn, J. Appl. Phys. **86**, 4997 (1999).

13. D.J. Lockwood, J. Solut. Chem. **29**, 1039 (2000).

14. N. Dmitruk, S. Kutovyi, I. Dmitruk, I. Simkiene, J. Sabataityte, and N. Berezovska, Sensors Actuat. B–Chem. **126**, 294 (2007).

15. N. Dmitruk, T Barlas, I. Dmitruk, S. Kutovyi, N. Berezovska, J. Sabataityte, and I. Simkiene, Phys. Status Solidi B **247**, 955 (2010).

16. R.W. Tjerkstra, Electrochem. Solid-State Lett. **9**, C81 (2006).

17. Shu-Lin Zhang, Yongtian Hou, Kuok-San Ho, Bidong Qian, and Shengmin Cai, J. Appl. Phys. **72**, 4469 (1992).

18. D.J. Lockwood, Guolin Yu, and N.L. Rowell, Solid State Commun. **136**, 404 (2005).

19. O. Madelung, *Semiconductors: Group IV Elements and III-V Compounds* (Springer, Berlin, 1991).

20. N.L. Dmitruk, A.V. Goncharenko, and E.F. Venger, *Optics of Small Particles and Composite Media* (Naukova Dumka, Kyiv, 2009).

21. Y.J. Chen, E. Barstein, and D.L. Mills, Phys. Rev. Lett. **34**, 1516 (1975).

22. A. Liu and C. Duan, Physica E **9**, 723 (2001).

23. G. Irmer, J. Raman Spectrosc. **38**, 634 (2007).

24. Y. Kayanuma, Phys. Rev. B **38**, 9797 (1988).

25. S. Adachi, *Physical Properties of III-V Semiconductor Compounds: InP, InAs, GaAs, GaP, InGaAs, and InGaAsP* (Wiley, New York, 1992).

26. A. Liu and C. Duan, Solid-State Electron. **45**, 2089 (2001).

27. G. Su, Q. Guo, and R.E. Palmer, J. Appl. Phys. **94**, 7598 (2003).

28. H. Hasegawa and T. Sato, Electrochim. Acta **50**, 3015 (2005).

29. A.A. Sitnikova, A.V. Bobyl, S.G. Konnikov, and V.P. Ulin, Semicond. **39**, 523 (2005).

30. D.N. Goryachev, L.V. Belyakov, and O.M. Sreseli, Semicond. **44**, 1588 (2010).

МОДИФІКАЦІЯ ОПТИЧНИХ ВЛАСТИВОСТЕЙ ПОРИСТИХ ШАРІВ НАПІВПРОВІДНИКІВ $A^{III}B^{V}$, ОТРИМАНИХ МЕТОДОМ АНОДНОГО ТРАВЛЕННЯ

М.Л. Дмитрук, Н.І. Березовська, І.М. Дмитрук, В.О. Сердюк, Дж. Сабатайтіте, І. Сімкіене

Р е з ю м е

Дослідження морфології поверхні (за допомогою атомно-силової мікроскопії (АСМ) та скануючої електронної мікроскопії (СЕМ)), комбінаційного розсіювання світла (КРС) та фотолюмінесценції (ФЛ) проведено з метою охарактеризувати серію матеріалів типу $A^{III}B^{V}$ (GaAs, GaP, InP) з пористою поверхнею, отриманою за допомогою методу електрохімічного травлення. Було показано, що морфологія поверхні пористих шарів сполук $A^{III}B^{V}$ суттєво залежить від різних параметрів процесу анодування, таких як час травлення, щільність струму, склад розчину травника і наявність освітлення під час травлення. Підсилення сигналу в спектрах КРС від пористої поверхні спостерігається майже у всіх досліджених зразках, що пояснюється, головним чином, порушенням правил відбору для відповідних фононних мод і зменшенням відбивання від пористої поверхні. Особливості спектрів ФЛ пористих сполук $A^{III}B^{V}$ вивчались в широкому температурному діапазоні. Для пористих поверхонь GaAs і InP спостерігався незначний квантово-розмірний ефект.